

# Inclusive breakup calculations in angular momentum basis: application to ${}^7\text{Li}+{}^{58}\text{Ni}$

Jin Lei<sup>1,\*</sup>

<sup>1</sup>*Institute of Nuclear and Particle Physics, and Department of Physics and Astronomy, Ohio University, Athens, Ohio 45701, USA*

(Dated: October 12, 2018)

The angular momentum basis method is introduced to solve the inclusive breakup within the model proposed by Ichimura, Austern, and Vincent [Phys. Rev. C 32, 431 (1985)]. This method is based on the geometric transformation between Jacobi coordinates, thus it is easy to incorporate with particle spins. To test the validity of this partial wave expansion method, a benchmark calculation is done comparing with the one given in [Phys. Rev. C 92, 044616 (2015)]. Using the distorted-wave Born approximation (DWBA) version of IAV model, some applications to  ${}^7\text{Li}$  reactions are presented and compared with available data.

## I. INTRODUCTION

Investigation of mechanisms responsible for the large inclusive  $\alpha$  particle production cross section observed in breakup of light-weakly bound projectiles (e.g.  ${}^6,8\text{He}$ ,  ${}^6,7\text{Li}$  and  ${}^7,9\text{Be}$ ) is a topic of current interest, both experimentally and theoretically [1–5]. This is a difficult problem, because different reaction mechanisms, like elastic breakup, transfer, compound nuclear evaporation, inelastic breakup and incomplete fusion contribute to the  $\alpha$  yield.

From the theoretical point of view, one can represent this kind of reactions as  $a + A \rightarrow b + B^*$ , where  $a = b + x$  and  $B^*$  is any possible state of  $x + A$  system. This reaction includes the breakup processes in which  $x$  is elastically scattered by  $A$  leaving all the fragments in the ground states, which is usually called elastic breakup (EBU), but also breakup accompanied by target excitation, particle(s) exchange between  $x$  and  $A$ ,  $x$  transfer to  $A$ , the fusion of  $x$  by  $A$ , which are globally referred to as nonelastic breakup (NEB). The total breakup (TBU) is therefore the sum of EBU and NEB components.

The IAV model [6], which was originally proposed in the 1980s, is used to study this inclusive breakup. Due to the computational limitations at that time, this model was apparently fallen into disuse. Recently, the model has been re-examined by several groups [7–12]. Moreover a systematic study of the alpha productions in  ${}^6\text{Li}$  induced reactions has been recently reported by Lei and Moro [13], in which the numerical calculations using the IAV model agree well with the experimental data.

For  ${}^7\text{Li}$ , several experimental groups have reported large alpha yields and tried to understand the origins of these alphas by using Q-value considerations and by direct identification of the reaction products [2, 14–16]. However, a proper interpretation of these alphas are still lacking. The IAV model, which successfully reproduce the alphas produced by  ${}^6\text{Li}$  is a promising tool for this purpose. From the theoretical point of view, a important difference between these two systems is that the

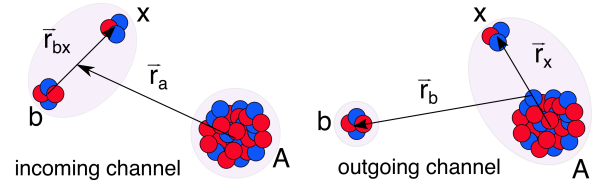


FIG. 1. (Color online) Coordinates used in the breakup reaction.

$\alpha + d$  cluster in  ${}^6\text{Li}$  is in a predominantly  $\ell = 0$  configuration, whereas the  $\alpha + t$  cluster conforming the  ${}^7\text{Li}$  system is in a  $\ell = 1$  configuration. This makes the numerical calculation more challenging since more angular momentum configurations are involved in the calculation.

For this reason, most applications of the IAV formalism have been restricted to deuterons and  ${}^6\text{Li}$ . In order to extend the model to other interesting systems, it is advisable to test its validity and accuracy for  $\ell > 0$  cases.

In the paper, a new method to compute the IAV inclusive breakup formula is implemented in a more efficient way. The derived formula has been tested for the  $\ell = 0$  against the previously implemented method. This former method becomes numerically difficult for  $\ell > 0$  cases, due to the additional angular momentum couplings (details see Appendix B of Ref.[7]). Moreover, the inclusion of the intrinsic spins will make the calculation even harder. Consequently, an alternative method which can deal with these more complicated situations would be advisable.

The paper is organized as follows: In Sec. II we summarize the main formulas of the IAV model and outline expansion in angular momentum basis. In Sec. III, the formalism is applied to inclusive breakup reactions induced by  ${}^7\text{Li}$ . Finally, in Sec. IV we summarize the main results.

## II. THEORETICAL MODELS

In this section, we briefly summarize the model of IAV and introduce a more efficient method for partial wave expansion comparing with the one used in Ref.[7]. The new

\* jinl@ohio.edu

method is more general and easy to incorporate particle spins.

First, we can write the process under study in the form

$$a(= b + x) + A \rightarrow b + B^*, \quad (1)$$

where the projectile  $a$ , constituted by  $b$  and  $x$ , interacts with the target  $A$ , leaving particle  $b$  and other fragments. Thus  $B^*$  is any possible state between  $x + A$  system.

The effective three body Hamiltonian of this system is

$$H(\xi) = H_0 + V_{bx} + V_{xA}(\xi) + U_{bA} + H_A(\xi), \quad (2)$$

where  $H_0$  is the total kinetic energy operator,  $V_{bx}$  is the interaction between the cluster  $b$  and  $x$ ,  $H_A(\xi)$  is the Hamiltonian of the target nucleus (with  $\xi$  denoting its internal coordinates), and  $V_{xA}$  and  $U_{bA}$  are fragment-target interactions.

In writing the Hamiltonian of the system in the form (2) we make a clear distinction between the two cluster constituents; the interaction with the target of the fragment  $b$ , the one which is assumed to be observed in the experiment, is described with a (complex) optical potential. Nonelastic processes arising from this interaction (e.g., target excitation, transfer, sequential breakup, and incomplete fusion) are included only effectively through the imaginary part of  $U_{bA}$ . Then particle  $b$  is said to act as a spectator. On the other hand, the interaction of the particle  $x$  with the target retains the target degrees of freedom ( $\xi$ ).

By using the closure relation and optical reduction, IAV separated the inclusive breakup cross section in terms of elastic breakup and nonelastic breakup, with the latter is given by

$$\left. \frac{d^2\sigma}{dE_b d\Omega_b} \right|_{NEB} = -\frac{2}{\hbar\nu_a} \rho_b(E_b) \langle \psi_x^0(\vec{k}_b) | W_x | \psi_x^0(\vec{k}_b) \rangle, \quad (3)$$

where  $\nu_a$  is the projectile-target relative velocity,  $\rho_b(E_b) = k_b \mu_b / [(2\pi)^3 \hbar^2]$  is the density of the states for the projectile  $b$ ,  $W_x$  is the imaginary part of the optical potential describing  $x + A$  elastic scattering, and  $\psi_x^0(\vec{k}_b)$  is the relative state between  $x$  and  $A$ , which governs the evolution of  $x$  after the collision, when particle  $b$  is emitted with momentum  $\vec{k}_b$  and the target remains in its ground state. This states satisfies the following equation when representing on  $x - A$  relative coordinates  $\vec{r}_x$ , where the relevant coordinates are depicted in Fig. 1

$$\langle \vec{r}_x | \psi_x^0(\vec{k}_b) \rangle = \int_0^\infty d\vec{r}'_x G_x(\vec{r}_x, \vec{r}'_x) \langle \vec{r}'_x | \chi_b(\vec{k}_b) | V_{\text{post}} | \Psi^{3b} \rangle, \quad (4)$$

where  $G_x = 1/(E_x - H_x)$  with the internal Hamiltonian  $H_x = T_x + U_x$  of  $x - A$  subsystem and the relative energy  $E_x$  between particles  $x$  and  $A$ ,  $\chi_b$  is the distorted-wave describing the scattering of  $b$  in the final channel with respect to the  $x - A$  subsystem,  $V_{\text{post}} = V_{bx} + U_{bA} - U_b$  (with  $U_b$  the optical potential in the outgoing channel) and  $\Psi^{3b}$  is the three-body wave function, with boundary conditions corresponding to the incident  $a$  particle.

Austern *et al.* [17] suggested using the CDCC wave function to approximate the three-body wave function,  $\Psi^{3b}$ , appearing in Eq.(4). Since the CDCC wave function is also a complicated object which contains different partial wave components for the  $b - x$  subsystem, one needs to treat each partial wave equally. In previous works[7, 13], we have tested the validity of  $\ell = 0$  case (deuterons and  ${}^6\text{Li}$ ) and compared the calculation results with experimental data. However, the IAV model has never been applied and tested for  $\ell \geq 1$  cases to our knowledge. For that purpose, we employ the distorted-wave Born approximation (DWBA), i.e.,  $\Psi^{3b} = \chi_a^{(+)} \phi_a$ , where  $\chi_a^{(+)}$  is the distorted wave describing the  $a + A$  elastic scattering and  $\phi_a$  is the projectile ground state wave function. Here we will focus on  $\ell = 1$  case with  ${}^7\text{Li}$ .

Instead of using a three dimensional Jacobi basis, we expand the wave function into partial wave eigenstates which depend on the magnitude of the radius and angular momentum eigenstates. The orbital angular momenta of three particles are coupled to total angular momentum  $J$  and its third component, for the incoming channels

$$|r_{bx} r_a \alpha_{in}\rangle = |r_{bx} r_a ((l_a(j_b j_x) s_{bx}) J_a(\lambda_a j_A) J_A) J M J\rangle_{in}, \quad (5)$$

and for the outgoing channels

$$|r_x r_b \alpha_{out}\rangle = |r_x r_b ((l_x(j_x j_A) s_{xA}) J_x(\lambda_b j_b) J_b) J M J\rangle_{out}, \quad (6)$$

where  $j_b$ ,  $j_x$  and  $j_A$  are the internal spins of particles  $b$ ,  $x$ , and  $A$  respectively and  $l_a$ ,  $\lambda_a$ ,  $l_x$ , and  $\lambda_b$  are the relative angular momentum of  $b - x$ ,  $a - A$ ,  $x - A$ , and  $b - B^*$  respectively.

The angular momentum basis can be normalized as,

$$\langle r'_{bx} r'_a \alpha'_{in} | r_{bx} r_a \alpha_{in} \rangle = \frac{\delta(r'_{bx} - r_{bx}) \delta(r'_a - r_a)}{r'_{bx} r_{bx} r'_a r_a} \delta_{\alpha'_{in}, \alpha_{in}}, \quad (7)$$

and likewise for the outgoing basis.

In addition to that, a two body angular momentum basis for the  $x - A$  subsystem is used,

$$|r_x \beta\rangle = |r_x (l_x s_{xA}) J_x M_x\rangle, \quad (8)$$

therefore, the three body outgoing state can be decoupled by

$$|r_x r_b \alpha_{out}\rangle = \sum_{M_x M_b} \langle J_x M_x J_b M_b | J M J \rangle |r_x \beta\rangle |r_b J_b M_b\rangle, \quad (9)$$

as well as the incoming state

$$|r_{bx} r_a \alpha_{in}\rangle = \sum_{M_a M_A} \langle J_a M_a J_A M_A | J M J \rangle |r_{bx} J_a M_a\rangle |r_a J_A M_A\rangle, \quad (10)$$

where  $M_x$ ,  $M_b$ ,  $M_a$ , and  $M_A$  are the third component of  $J_x$ ,  $J_b$ ,  $J_a$ , and  $J_A$  respectively.

By using the angular momentum basis defined above,

we can rewrite Eq.(4) as

$$\langle r_x \beta | \psi_x^0(\vec{k}_b) \rangle = \int_0^\infty dr'_x r_x'^2 G_x(r_x, r'_x, \beta) \rho(r'_x, \beta, \vec{k}_b), \quad (11)$$

with

$$\rho(r'_x, \beta, \vec{k}_b) = \langle r'_x \beta \chi_b^{(-)}(\vec{k}_b) | V_{\text{post}} | \chi_a^{(+)} \phi_a \rangle. \quad (12)$$

Since the incoming and outgoing channels are repre-

sented in their natural set of Jacobi coordinate(see Fig.1). A transformation from the sets  $|r_{bx}r_a\alpha_{in}\rangle$  to  $|r_xr_b\alpha_{out}\rangle$  is required. A partial wave representation of this transformation is outlined in Ref.[18] and can be written as an integration over the cosine of the relative angle between  $\vec{r}_x$  and  $\vec{r}_b$ . All geometrical information is included in the coefficients  $\mathcal{G}_{\alpha_{in},\alpha_{out}}^{\text{out}\leftarrow\text{in}}(r_xr_bx)$ . We give more details on these transformation in Appendix A. Additionally, we only consider a central potential for  $U_{bA}$ . Then inserting complete set of states in Eq. (13) and making use of the geometrical coefficients  $\mathcal{G}_{\alpha_{in},\alpha_{out}}^{\text{out}\leftarrow\text{in}}(r_xr_bx)$ , we arrive at the following equation:

$$\rho(r'_x, \beta, \vec{k}_b) = \sum_{\alpha_{out}} \int_0^\infty dr'_x r_x'^2 \langle r'_x \beta \chi_b^{(-)}(\vec{k}_b) | r'_x r'_b \alpha_{out} \rangle \sum_{\alpha_{in}} \int_{-1}^1 dx V_{\text{post}}(r'_x r'_b x \alpha_{out}) \mathcal{G}_{\alpha_{in},\alpha_{out}}^{\text{out}\leftarrow\text{in}}(r'_x r'_b x) \langle r_{bx} r_a \alpha_{in} | \chi_a^{(+)} \phi_a \rangle, \quad (13)$$

with

$$\langle r'_x \beta \chi_b^{(-)}(\vec{k}_b) | r'_x r'_b \alpha_{out} \rangle = \sum_{M_x M_b} \langle J_x M_x J_b M_b | J M J \rangle \langle \chi_b^{(-)}(\vec{k}_b) | r_b J_b M_b \rangle \delta_{\beta, J_x M_x}, \quad (14)$$

and

$$\langle r_{bx} r_a \alpha_{in} | \chi_a^{(+)} \phi_a \rangle = \sum_{M'_a M_A} \langle J_a M'_a J_A M_A | J M J \rangle \langle r_{bx} J_a M'_a | \phi_a \rangle \langle r_a J_A M_A | \chi_a^{(+)} \rangle, \quad (15)$$

The double differential cross section of NEB, which

given by Eq. (3) can be represented with the angular momentum basis as

$$\left. \frac{d^2\sigma}{dE_b d\Omega_b} \right|_{NEB} = -\frac{2}{\hbar\nu_a} \rho_b(E_b) \sum_{\beta} \int_0^\infty dr_x r_x^2 |\psi_x^0(r_x, \beta, \vec{k}_b)|^2 W_x(r_x, \beta). \quad (16)$$

We consider the case of unpolarized beam, and aligned target. Moreover, we assume that the spin orientation of  $b$  is not measured. In this situation, the cross section

is obtained as an average of the initial angular momentum projections of  $J_a$  and  $J_A$ , and a sum over the final projection of  $J_b$ . Thus

$$\left. \frac{d^2\sigma}{dE_b d\Omega_b} \right|_{NEB} = -\frac{2}{\hbar\nu_a} \rho_b(E_b) \frac{1}{(2J_a + 1)(2J_A + 1)} \sum_{\beta} \sum_{M_a m_A m_b} \int_0^\infty dr_x r_x^2 |\psi_x^0(r_x, \beta, \vec{k}_b)|^2 W_x(r_x, \beta). \quad (17)$$

where  $m_A$  and  $m_b$  are the third components of  $j_A$  and

$j_b$ , respectively

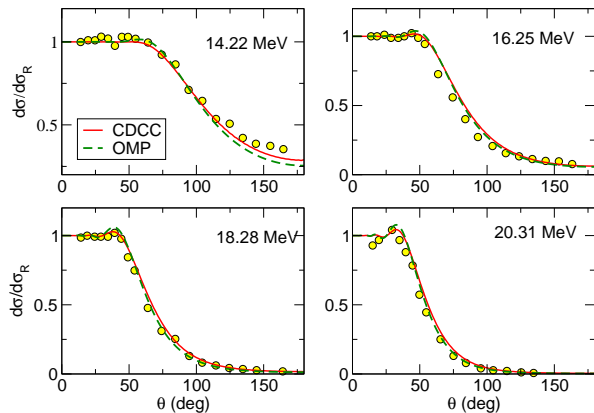


FIG. 2. (Color online) Elastic scattering of  ${}^7\text{Li} + {}^{58}\text{Ni}$  at different incident energies. The solid and dashed lines are the CDCC calculations and the optical model calculation with the OMP of Cook [19], respectively. Experimental data are taken from Ref. [20].

### III. CALCULATIONS

#### A. ${}^{58}\text{Ni}({}^7\text{Li}, \alpha X)$

To assess the validity of this partial wave expansion, we have done the benchmark calculation comparing our earlier expansion given in Ref. [7]. The numerical difference between these two methods is less than 1% by using the same input parameters. On the other hand, the well-known convergence problem in DWBA post form makes  $\rho^{M_\alpha}(r'_x, \beta)$  of Eq. (13) long ranged. To overcome this issue, an identical prior form [8] is used.

Now we present calculations for reactions induced by a  ${}^7\text{Li}$  projectile and compare the calculated inclusive cross sections with experimental data to assess the validity of the theory. In this case, we compute the separate contributions for the elastic (EBU) and nonelastic (NEB) breakup cross sections. For the former, we use the CDCC formalism, using the coupled-channels code FRESKO[21]. This makes it possible to treat the EBU to all orders and should be equivalent to the post-form three-body model of Austern et al. For the NEB part, we use the DWBA version.

We consider the reaction  ${}^{58}\text{Ni}({}^7\text{Li}, \alpha X)$  at energies around Coulomb barrier, which allows us to compare with data from Ref.[20]. The  ${}^7\text{Li}$  nucleus is treated in a two-cluster model ( $\alpha + t$ ). Compared to the ( $\alpha + d$ ) two-cluster structure of  ${}^6\text{Li}$ , the main difference between the two nuclei is the internal angular momentum  $\ell$ , for  ${}^6\text{Li}$   $\ell = 0$ , whereas for  ${}^7\text{Li}$   $\ell = 1$ . Furthermore the difference in the breakup threshold energy of the two Li isotopes, 1.474 MeV for  $\alpha + d$  breakup of  ${}^6\text{Li}$  compared to 2.468 MeV for the  $\alpha + t$  breakup of  ${}^7\text{Li}$  is also important.

In order to test the validity of the  $\alpha + t$  two cluster model for  ${}^7\text{Li}$ , first the elastic scattering of the same reaction was studied using the CDCC framework. The  $\alpha + t$

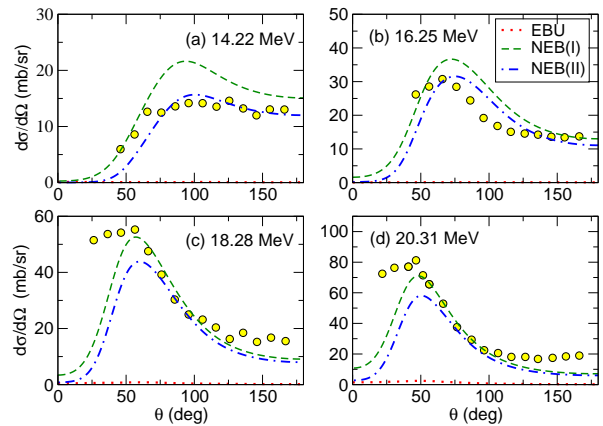


FIG. 3. (Color online) Angular distribution of  $\alpha$  particles produced in the reaction  ${}^7\text{Li} + {}^{58}\text{Ni}$  at energies indicated by the labels. The dotted, dashed and dot-dashed are, respectively, the EBU, NEB (DWBA) with  $E_x < 0$ , and NEB (DWBA) without  $E_x < 0$  components. The experimental data are taken from Ref. [20].

interaction, which is required to generate the  ${}^7\text{Li}$  ground state wave function as well as the bound excited state and continuum wave functions, was taken from Ref.[22]. This potential consists of a central and a spin-orbit component, of Gaussian shape, with a fixed geometry and a parity-dependent depth. The potential well depths were adjusted to give the correct binding energy or resonance energy for bound or resonant states, respectively. In order to achieve convergence of the calculated cross sections, we needed to include  $\alpha + t$  partial waves up to  $\ell = 3$ . For the  $f$  wave, a finer division of bins is used in order to reproduce the  $\ell = 3$  resonant states at 4.63 MeV ( $7/2^-$ ) and 6.68 MeV ( $5/2^-$ ) correctly. The  ${}^4\text{He}$ -target interaction was obtained from a Woods-Saxon potential fitted to the 12 MeV  ${}^4\text{He} + {}^{58}\text{Ni}$  elastic scattering data of Ref.[23] with the following parameters :  $V = 49.5$  MeV,  $R_0 = 5.88$  fm,  $a_0 = 0.5$  fm,  $W = 11.0$  MeV,  $R_w = 5.69$  fm and  $a_w = 0.5$  fm. The  ${}^3\text{He}$ -target interaction was taken from the 8.95 MeV  $t + {}^{58}\text{Ni}$  parameters of Ref.[24]. For comparison, the optical model calculation using the potential of Cook[19] was also performed. Fig. 2 shows the elastic scattering of  ${}^7\text{Li} + {}^{58}\text{Ni}$  at different incident energies. The data are taken from Ref.[20]. The solid and dashed lines are, respectively, the CDCC and optical model calculations. It can be seen that both the optical model and CDCC calculations reproduce well the experimental data. This agreement confirms the validity of the adopted  $\alpha$ -target and  $t$ -target optical potentials.

Now the inclusive breakup cross section ( ${}^7\text{Li}, \alpha X$ ) is discussed. The EBU part was obtained from the CDCC calculation discussed above. The NEB part was calculated with the IAV model using the DWBA formalism without taking account the spin of particles. There are two distinct contributions to the NEB cross sections, namely, that for  $E_x > 0$  case and that for  $E_x < 0$  case,

where  $E_x$  is the final relative energy between  $t$  and  $^{58}\text{Ni}$ . For  $E_x < 0$ , this region would correspond to bound states of the residual  $^{61}\text{Cu}$  system, that is, transfer. The application of NEB formalism to transfer reactions is outlined in Ref.[25] and recently applied to deuterons and  $^6\text{Li}$  induced reactions[13, 26]. In Fig. 3 the dotted, dashed and dot-dashed lines are, respectively, the EBU (CDCC), NEB (DWBA) with  $E_x < 0$ , and NEB (DWBA) without  $E_x < 0$  components. First, it is noticeable that the EBU part is negligible compared to the NEB component, which is in contrast to  $^6\text{Li}$  as reported in Ref.[13]. For the  $^6\text{Li}$  case, the contribution of EBU is small but non-negligible comparing to NEB. The difference of these two nuclei will be discussed in the following section. Concerning the comparison of the calculations with experimental data, we observe a good agreement with the data when including the  $E_x < 0$  part for higher two energies and excluding the  $E_x < 0$  for lower two energies. The reason of that is not completely clear but it might be due to the fact that an energy-independent  $t+^{58}\text{Ni}$  potential has been employed, which will not describe correctly the low energy region (including the bound state part) of this system. A more realistic description should be provided by a energy-dependent potential, extending also to negative energies. Such potentials were investigated in the past by Mahaux and Sartor [27] and are currently being revisited by several groups (see Ref. [28] for a recent review).

### B. Comparison with the $^6\text{Li}$ case

In this section, the difference between  $^6\text{Li}$  and  $^7\text{Li}$  on the  $^{58}\text{Ni}$  target is discussed. The calculations of  $^6\text{Li}$  have been presented in Ref.[13] In both cases, we have found that the NEB<sup>1</sup> component dominates the inclusive alphas. However it is interesting to compare the relative importance of EBU versus NEB on these two nuclei. In order to make a more meaningful comparison with these two nuclei, a toy model of  $^6\text{Li}$  is introduced by modifying the binding energy from  $E_b = -1.474$  MeV to  $E_b = -2.468$  MeV (that is, the  $^7\text{Li}$  binding energy). Fig.4 (a) plots the ratio of the calculated EBU and TBU (=EBU+NEB) cross section as a function of the reduced energy  $E_{c.m.}/V_B$ , with  $V_B$  the energy of the Coulomb barrier, estimated as  $V_B = Z_p Z_t / [r_B (A_t^{1/3} + A_p^{1/3})]$ , where  $Z_p(Z_t)$  and  $A_p(A_t)$  are the atomic number and atomic mass of projectile (target), respectively, and  $r_B = 1.44$  fm. The circles, squares and diamonds are respectively  $^6\text{Li} + ^{58}\text{Ni}$ ,  $^6\text{Li}^{\text{toy}} + ^{58}\text{Ni}$  and  $^7\text{Li} + ^{58}\text{Ni}$  reaction systems. Several interesting features emerge from this plot: (i) First, for the lower binding energy, i.e.,  $^6\text{Li} + ^{58}\text{Ni}$ , the elastic breakup component becomes more important as the energy decreases, whereas for the energies above

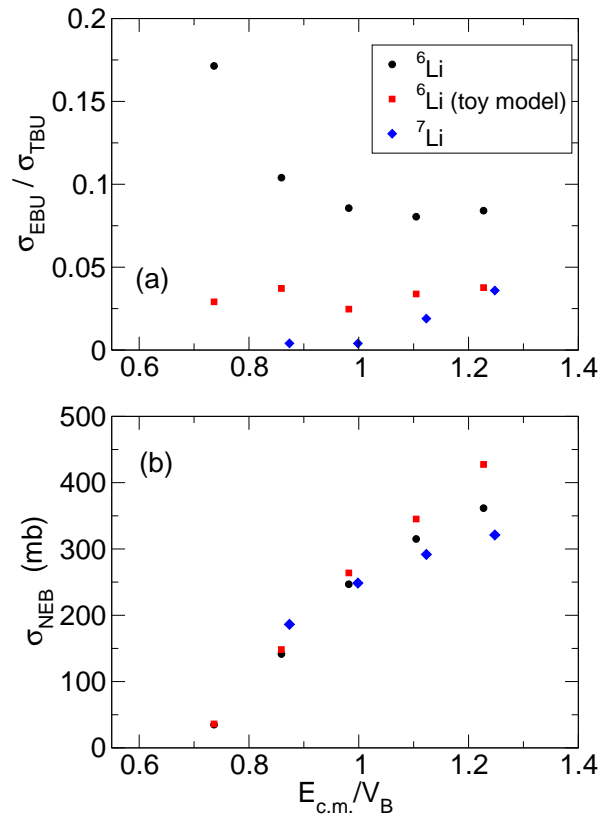


FIG. 4. (Color online) (a) Ratios of EBU over TBU (=EBU+NEB) for  $^{6,7}\text{Li} + ^{58}\text{Ni}$  systems. (b) NEB cross sections for  $^{6,7}\text{Li} + ^{58}\text{Ni}$  systems. See text for details.

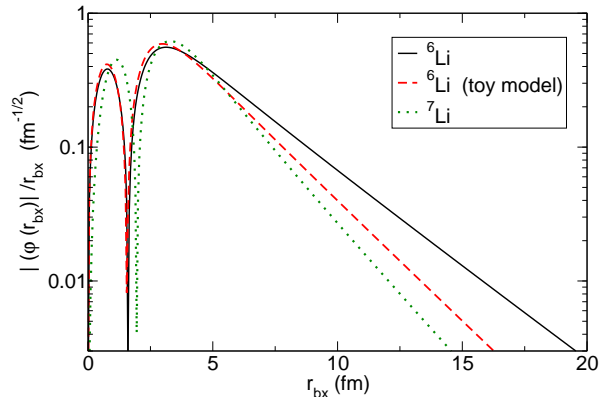


FIG. 5. (Color online) Projectile wave functions for  $^{6,7}\text{Li}$ . See text for details.

the Coulomb barrier, the ratio shows an almost constant behavior; (ii) second, when increasing the binding of projectile, i.e.,  $^6\text{Li}^{\text{toy}} + ^{58}\text{Ni}$ , the elastic breakup component becomes comparatively smaller; (iii) third, when changing the relative angular momentum in the projectile from  $\ell = 0$  to  $\ell = 1$ , i.e.,  $^7\text{Li} + ^{58}\text{Ni}$ , the importance of elastic breakup component increases with the incident energy. These results can be attributed to the fact that the EBU

<sup>1</sup> NEB means the one with both  $E_x > 0$  and  $E_x < 0$  components

is a peripheral process and thereby highly sensitive to the tail of projectile wave function. In Fig. 5, it can be clearly seen that  ${}^6\text{Li}$  has the longest tail among these three systems and this explains the larger EBU contribution. By contrast, since the wave function of  ${}^7\text{Li}$  is deeper hidden inside the Coulomb force, this case the  ${}^7\text{Li}$  projectile difficult to break in the relative low energies.

Fig.4 (b) shows the NEB cross sections as a function of the reduced energy  $E_{c.m.}/V_B$ . It can be seen that the NEB cross section for these three systems are of similar magnitude. The NEB cross sections increase when changing the projectile binding energy by comparing with  ${}^6\text{Li} + {}^{58}\text{Ni}$  and  ${}^6\text{Li}^{\text{to}y} + {}^{58}\text{Ni}$ . However, the NEB cross section decrease when changing the internal relative angular momentum from  $\ell = 0$  to  $\ell = 1$  ( ${}^6\text{Li}^{\text{to}y}$  to  ${}^7\text{Li}$ ). These behaviors indicate that the NEB is a volume process which comes from the interior part of projectile wave function and less sensitive to the internal structure of the projectile. This agrees with the fact that found in Ref. [12].

#### IV. SUMMARY AND CONCLUSIONS

In summary, we addressed the problem of calculating the inclusive breakup cross section for arbitrary  $\ell$  values (with  $\ell$  the orbital angular momentum between the clusters in the projectile ground state) within the closed-form DWBA model proposed in the 1980s by Ichimura,

Austern, and Vincent[6]. Moreover, numerical implementation of the model, more suitable for  $\ell > 0$  values, has been presented here.

We have performed calculations for the  ${}^{58}\text{Ni}({}^7\text{Li},\alpha X)$  at energies around the Coulomb barrier. In this case, we find a good agreement between the experimental data and the IAV model.

We also investigated effect of the internal structure of the projectile by comparing the  ${}^7\text{Li}$  inclusive breakup with  ${}^6\text{Li}$ . Although in both cases the  $\alpha$  inclusive cross section is dominated by the NEB component, the EBU part is comparatively larger for the  ${}^6\text{Li}$  case. We interpret this as a consequence of the larger extension of the  ${}^6\text{Li}$  ground state wave function, due to its  $\ell = 0$  configuration.

The results presented in this work, along with those presented in previous works[7, 8, 13], indicate that the IAV model provides a reliable framework to calculate NEB cross sections. Possible applications to knockout reactions at intermediate energies are currently under study.

#### Appendix A: Geometrical coefficient for coordinate transformation

In this section, we present the explicit expressions of the geometrical coefficients  $\mathcal{G}_{\alpha_{in},\alpha_{out}}^{\text{out}\leftarrow\text{in}}(r'_x r'_b x)$ . These are given by

$$\begin{aligned} \mathcal{G}_{\alpha_{in},\alpha_{out}}^{\text{out}\leftarrow\text{in}}(r'_x r'_b x) &= \sum_{LS} (2S+1) \sqrt{(2J_a+1)(2J_A+1)(2J_x+1)(2J_b+1)} \begin{Bmatrix} l_x & s_{xA} & J_x \\ \lambda_b & j_b & J_b \\ L & S & J \end{Bmatrix} \begin{Bmatrix} l_a & s_{bx} & J_a \\ \lambda_a & j_A & J_A \\ L & S & J \end{Bmatrix} \\ &\times 8\pi^2 \sum_{M=-L}^L \left\{ Y_{l_x}^{m_{l_x^*}}(\hat{r}_x) Y_{\lambda_b}^{m_{\lambda_b^*}}(\hat{r}_b) \right\}^{LM} \left\{ Y_{l_a}^{m_{l_a}}(\widehat{a\vec{r}_x - \vec{r}_b}) Y_{\lambda_a}^{m_{\lambda_a}}(\widehat{b\vec{r}_x + c\vec{r}_b}) \right\}^{LM} \\ &\times (-)^{s_{bx}+2j_A+j_x+j_b} \sqrt{(2s_{xA}+1)(2s_{bx}+1)} \begin{Bmatrix} j_A & j_x & s_{xA} \\ j_b & S & s_{bx} \end{Bmatrix}. \end{aligned} \quad (\text{A1})$$

The spherical harmonics  $Y_l^m(\hat{r})$  depend on the angles  $\hat{r}$  of the vector  $\vec{r}$ . For the evaluation, we choose  $\vec{r}_b$  as  $z$ -direction and  $\vec{r}_x$  is in the  $x-y$  plane:

$$\vec{r}_b = \begin{pmatrix} 0 \\ 0 \\ r_b \end{pmatrix} \quad \vec{r}_x = \begin{pmatrix} r_x \sqrt{1-x^2} \\ 0 \\ r_x x \end{pmatrix}, \quad (\text{A2})$$

where  $x$  is the cosine of the angle between  $\vec{r}_b$  and  $\vec{r}_x$ . In Eq. (A1) the curly brackets grouping the spherical harmonics indicate that they are coupled to a state of total orbital angular momentum  $L$  and third component

$M$ . The mass ratios are given by

$$\begin{aligned} a &= \frac{m_A}{m_A + m_x} \\ b &= \frac{(m_b + m_x + m_A) m_x}{(m_A + m_x)(m_b + m_x)} \\ c &= \frac{m_b}{m_b + m_x}. \end{aligned} \quad (\text{A3})$$

For this case, the coordinates of the incoming channel are given by

$$\begin{aligned} r_{bx}(r_x r_b x) &= \sqrt{a^2 r_x^2 + r_b^2 - 2ar_x r_b x} \\ r_a(r_x r_b x) &= \sqrt{b^2 r_x^2 + c^2 r_b^2 + 2bcr_x r_b x}. \end{aligned} \quad (\text{A4})$$

## ACKNOWLEDGMENTS

The author is grateful to Antonio M. Moro and Filomena Nunes for a critical reading of the manuscript and helpful discussions. This work has been supported by the National Science Foundation under contract. No. NSF-PHY-1520972 with Ohio University.

- 
- [1] D. Chattopadhyay, S. Santra, A. Pal, A. Kundu, K. Ramachandran, R. Tripathi, D. Sarkar, S. So-daye, B. K. Nayak, A. Saxena, and S. Kailas, *Phys. Rev. C* **94**, 061602 (2016).
- [2] S. K. Pandit, A. Shrivastava, K. Mahata, V. V. Parkar, R. Palit, N. Keeley, P. C. Rout, A. Kumar, K. Ramachandran, S. Bhattacharyya, V. Nanal, C. S. Palshetkar, T. N. Nag, S. Gupta, S. Biswas, S. Saha, J. Sethi, P. Singh, A. Chatterjee, and S. Kailas, *Phys. Rev. C* **96**, 044616 (2017).
- [3] P. Carnelli, D. M. Heimann, A. Pacheco, A. Arazi, O. Capurro, J. F. Niello, M. Cardona, E. de Barbar, J. Figueira, D. Hojman, G. Mart, and A. Negri, *Nuclear Physics A* **969**, 94 (2018).
- [4] O. Sgouros, A. Pakou, D. Pierroutsakou, M. Mazzocco, L. Acosta, X. Aslanoglou, C. Betsou, A. Boiano, C. Boiano, D. Carbone, M. Cavallaro, J. Grebosz, N. Keeley, M. La Commara, C. Manea, G. Marquinez-Duran, I. Martel, N. G. Nicolis, C. Parascandolo, K. Rusek, A. M. Sánchez-Benítez, C. Signorini, F. Soramel, V. Soukeras, C. Stefanini, E. Stiliaris, E. Strano, I. Strojek, and D. Torresi, *Phys. Rev. C* **94**, 044623 (2016).
- [5] L. Canto, P. Gomes, R. Donangelo, J. Lubian, and M. Hussein, *Physics Reports* **596**, 1 (2015), recent developments in fusion and direct reactions with weakly bound nuclei.
- [6] M. Ichimura, N. Austern, and C. M. Vincent, *Phys. Rev. C* **32**, 431 (1985).
- [7] J. Lei and A. M. Moro, *Phys. Rev. C* **92**, 044616 (2015).
- [8] J. Lei and A. M. Moro, *Phys. Rev. C* **92**, 061602 (2015).
- [9] G. Potel, F. M. Nunes, and I. J. Thompson, *Phys. Rev. C* **92**, 034611 (2015).
- [10] G. Potel, G. Perdikakis, B. V. Carlson, M. C. Atkinson, W. H. Dickhoff, J. E. Escher, M. S. Hussein, J. Lei, W. Li, A. O. Macchiavelli, A. M. Moro, F. M. Nunes, S. D. Pain, and J. Rotureau, *The European Physical Journal A* **53**, 178 (2017).
- [11] B. V. Carlson, R. Capote, and M. Sin, *Few-Body Systems* **57**, 307 (2016).
- [12] A. M. Moro and J. Lei, *Few-Body Systems* **57**, 319 (2016).
- [13] J. Lei and A. M. Moro, *Phys. Rev. C* **95**, 044605 (2017).
- [14] D. H. Luong, M. Dasgupta, D. J. Hinde, R. du Rietz, R. Rafiei, C. J. Lin, M. Evers, and A. Diaz-Torres, *Phys. Rev. C* **88**, 034609 (2013).
- [15] S. K. Pandit, A. Shrivastava, K. Mahata, N. Keeley, V. V. Parkar, P. C. Rout, K. Ramachandran, I. Martel, C. S. Palshetkar, A. Kumar, A. Chatterjee, and S. Kailas, *Phys. Rev. C* **93**, 061602 (2016).
- [16] A. Shrivastava, A. Navin, A. Diaz-Torres, V. Nanal, K. Ramachandran, M. Rejmund, S. Bhattacharyya, A. Chatterjee, S. Kailas, A. Lemasson, R. Palit, V. Parkar, R. Pillay, P. Rout, and Y. Sawant, *Physics Letters B* **718**, 931 (2013).
- [17] N. Austern, Y. Iseri, M. Kamimura, M. Kawai, G. Rawitscher, and M. Yahiro, *Physics Reports* **154**, 125 (1987).
- [18] R. Balian and E. Brézin, *Il Nuovo Cimento B (1965-1970)* **61**, 403 (1969).
- [19] J. Cook, *Nuclear Physics A* **388**, 153 (1982).
- [20] K. Pfeiffer, E. Speth, and K. Bethge, *Nuclear Physics A* **206**, 545 (1973).
- [21] I. J. Thompson, *Comp. Phys. Rep.* **7**, 167 (1988).
- [22] B. Buck and A. C. Merchant, *Journal of Physics G: Nuclear Physics* **14**, L211 (1988).
- [23] L. L. Lee and J. P. Schiffer, *Phys. Rev.* **134**, B765 (1964).
- [24] D. Fick, R. E. Brown, W. Grüebler, R. A. Hardekopf, and J. S. Hanspal, *Phys. Rev. C* **29**, 324 (1984).
- [25] T. Udagawa, Y. J. Lee, and T. Tamura, *Phys. Rev. C* **39**, 47 (1989).
- [26] G. Potel, G. Perdikakis, B. V. Carlson, M. C. Atkinson, W. H. Dickhoff, J. E. Escher, M. S. Hussein, J. Lei, W. Li, A. O. Macchiavelli, A. M. Moro, F. M. Nunes, S. D. Pain, and J. Rotureau, *The European Physical Journal A* **53**, 178 (2017).
- [27] C. Mahaux and R. Sartor, *Phys. Rev. Lett.* **57**, 3015 (1986).
- [28] W. H. Dickhoff, R. J. Charity, and M. H. Mahzoon, *Journal of Physics G: Nuclear and Particle Physics* **44**, 033001 (2017).